GIA®

NEWS FROM RESEARCH

Atypical Bead Cultured *Pinctada maxima* Pearls Nucleated with Freshwater Non-Bead Cultured Pearls

Promlikit Kessrapong and Kwanreun Lawanwong

Figure 1. The 12 white and "golden" South Sea cultured pearls (*Pinctada maxima*) of various shapes and sizes examined in this study. Although their external appearances are similar to saltwater bead and non-bead cultured (NBC) pearls, 11 of them are atypical bead cultured (aBC) pearls formed by inserting freshwater non-bead cultured pearls as nuclei into saltwater hosts. Photo by Nuttapol Kitdee.

Abstract

At present, most of the freshwater (FW) shell bead nuclei used in the cultured pearl industry originates from mussels fished in the Mississippi River, United States (Strack, 2006; Hsu et al., 2016). However, shell beads are not the only material used as nuclei in the culturing process. Cultured freshwater pearls have also been used as nuclei to produce atypical bead-cultured (aBC) South Sea pearls.

Twelve aBC pearl samples from Orient Pearl (Bangkok) Limited were examined with standard pearl testing methods. Microradiography and X-ray luminescence examination were applied to all the samples, while Raman and photoluminescence (PL) spectroscopy as well as ultraviolet visible spectrophotometry (UV-Vis) analyses were carried out on those of a "golden" hue. Two of the samples, one white and one "golden," were selected in order to cut in half and collect further data. The sawing enabled the X-ray luminescence of the inner overlying saltwater (SW) layers and freshwater pearl nuclei to be recorded and provided the opportunity to take additional photomicrographs and perform LA-ICP-MS chemical analysis across the inner surfaces of one half of each pearl.

As expected, the results on the two cut samples in particular confirmed their stated aBC nature. The internal structures revealed clear boundaries between the freshwater NBC pearl nuclei and the saltwater overgrowth layers. Raman, PL, and UV-Vis spectra for the "golden" sample indicated the pearl formed within a *Pinctada maxima* mollusk. Also, in keeping with their freshwater NBC nuclei structure, a weak to moderate fluorescence was observed in the intact samples, which would not be likely if they were entirely saltwater. The cut examples clearly showed that the strong fluorescence originated from the nuclei, as is the case with traditional (typical) bead cultured marine pearls in which freshwater shell nuclei are implanted. LA-ICP-MS analysis on the two cut samples clearly revealed the nature of the outer saltwater layers and inner freshwater pearls, thus confirming the fluorescence reactions and allowing clear identification of the chemical elements within the two components.

Standard pearl testing methods permit the straightforward identification of such aBC pearls. Cutting the pearls in half is a useful method to carry out further scientific examination in order to obtain more data not possible from the intact pearls.

o

Table of Contents

o

1.Introduction

White and yellow “golden” (Gemological Institute of America, 2011) South Sea cultured pearls are produced by the *Pinctada maxima* mollusk, which inhabits the waters of the Indian and Pacific Oceans (Strack, 2006). The leading sources of such pearls are Australia, Indonesia, the Philippines, and Myanmar. During the traditional bead culturing process, freshwater shell bead nuclei from North America are routinely inserted into mollusks. In this study, atypical bead cultured pearls in which freshwater non-bead cultured (NBC) pearls were reportedly inserted as nuclei are examined and described (figure 1). Most of the shell bead nuclei used in the cultured pearl industry originates from freshwater mussels (Sturman et al., 2016). However, shell beads are not the only material used as nuclei in the culturing process (Scarratt et al., 2017). As this work shows, cultured freshwater pearls have also been used as nuclei to produce atypical bead cultured (aBC) South Sea pearls. As would be expected, the external appearances of such pearls match cultured pearls produced by *Pinctada maxima* mollusks. However, misunderstandings may easily arise concerning the exact nature of the pearls, and hence their perceived value, if their true identity is not revealed by advanced testing. This work clearly illustrates the internal characteristics of this particular type of atypical bead cultured pearl.

2. Materials and methods

In 2017, 12 South Sea cultured pearl samples that had been produced using freshwater NBC pearl nuclei were obtained from Orient Pearl (Bangkok) Ltd. They were selected in person by GIA Thailand pearl researchers who had the opportunity to visit the company’s factory. The samples loaned were semi-baroque to baroque of white, light yellow, and strong yellow to strong orangy yellow colors. They weighed from 4.47 to 11.45 carats and ranged from 11.00 × 9.93 × 6.89 mm to 18.27 × 11.17 × 9.62 mm.

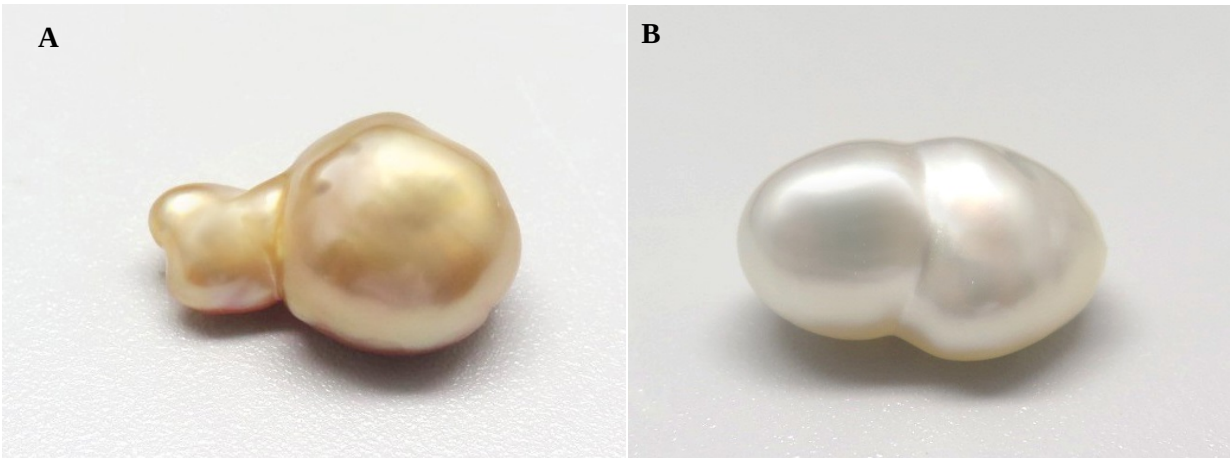

Figure 2. Two samples were selected for more detailed work. Each pearl was sawn in half at GIA’s field gemology department in Bangkok to study the internal structure. Pearl A (left) is orangy yellow and measures 18.27 × 11.17 × 9.62 mm, and pearl B (right) is white and measures 17.07 × 10.25 × 8.56 mm. Photos by Promlikit Kessrapong.

o

The internal structures of all the samples were examined with a Pacific X-ray Imaging (PXI) GenX-90P series real-time X-ray (RTX) unit with a 4-micron micro focus, 90 kV voltage and 0.16 mA current X-ray source, incorporating a PerkinElmer 4"/2" dual-view flat panel detector. A ProCon CT-mini X-ray system with a 5-micron micro focus, 90 kV voltage and 0.18 mA X-ray current source, and a Varex imaging flat panel detector with 74.8 µm pixel pitch were used to obtain X-ray computed microtomography data from three selected samples after reviewing the RTX results.

A FocalSpot Verifier PF-100 model FSX-PF100 X-ray fluorescence unit (voltage 100 kV and current 3.2 mA) was then used to provide information about the environment in which the pearl and nuclei formed, since marine and freshwater materials react differently when exposed to X-rays (Hänni et al., 2005).

Raman, PL, and UV-Vis spectroscopy analyses were carried out on the seven “golden” samples in the group (figure 1). An Agilent Cary 60 UV-Vis spectrophotometer utilizing a custom-made GIA integrated sphere accessory incorporating an 80 Hz xenon flash lamp source was used to collect spectra in the 200–800 nm range. A Renishaw inVia Reflex micro-Raman spectrometer system equipped with a 514 nm argon-ion laser was used to obtain Raman and PL spectra from the external and internal surfaces. The laser was set at 100% power utilizing three accumulations and an exposure time of 10 seconds. PL spectra were collected with the laser set at 50% power and utilizing one accumulation with an exposure time of 15 seconds.

The two samples selected for sawing (figure 2) were cut in half using a Lapcraft Dia-Laser diamond saw to reveal their internal structures. The surfaces were ground prior to polishing using a 600# diamond lap and then polished with a Smart Cut UKAM Industrial Superhard Tools lap and Light Side grit.

Photomicrography of the interior features of the two cut samples was performed using a Nikon SMZ18 microscope incorporating NIS-Elements imaging software.

Trace element chemistry results were obtained on one half of each sawn sample using a Thermo Fisher Scientific iCAP Qc inductively coupled plasma–mass spectrometer (ICP-MS) coupled with a Q-switched Nd:YAG laser ablation (LA) device operating at a wavelength of 213 nm. ICP-MS was operated using the forward power at ~1350 W and the typical nebulizer gas flow at ~0.80 L/min. Helium was used as the carrier gas in the laser ablation unit, and the flow rate was set at ~0.80 L/min. Laser conditions were 40 mm diameter laser spots, a fluence of around 10 J/cm^2, and a 10 Hz repetition rate. LA-ICP-MS analysis is a quasi-nondestructive method that creates small laser ablation spots throughout the testing area (Homkrajae et al., 2019).

o

3. Results and discussion

3.1 Real-time Microradiography

Real-time microradiographs of all 12 samples were obtained, and some of those related to the 10 intact pearls are shown in table 1. The results for the remaining two pearls that were subsequently selected for sawing (pearls A and B) and described in a preliminary work (Kessrapong and Lawanwong, 2018) are shown in table 2, together with photomicrographs in their sawn state. All the samples were X-rayed in at least three directions, two of which have been selected to show the internal structure of each sample in table 1. When the samples were analyzed side-on (table 1, left) they tended to reveal the clearest details with the demarcation between the nucleus and overlying nacre being most obvious in this orientation. An irregular demarcation outline between the nucleus and surrounding nacre, no obvious growth features in the overlying nacre, and twisted linear-like features typical of FW pearls (Scarratt et al., 2017) was shown in all but one of the samples. Experienced pearl testers may be able to accurately identify the environment in which a pearl formed from studying the internal RTX structures, especially NBC pearls, and as a result make a confident determination on the identity of a pearl as well. When, as in the majority of these pearls, there is an apparent mismatch of structures from one environment with the appearance and expected origin of another environment, concern about the true identity arises. The concerns become more pronounced when an irregular demarcation boundary appears in most of the samples. As has been discussed in the literature already, such demarcation boundaries are diagnostic of aBC pearls in which a variety of non-shell materials have been used as nuclei (Hänni et al., 2010; Scarratt et al., 2017).

However, the large void and organic-rich structure of pearl 6 (table 1) stands out from the structures of the others. Since there is no obvious demarcation boundary, it is clear that this pearl is either the odd one out in the group or, more likely, an NBC pearl (Sturman, 2009; Sturman et al., 2016; Nilpetploy et al., 2018).

o

Table 1. Macro images (left) of ten pearls, side-on oriented microradiography images (middle), and "facing view" (thinnest direction) oriented microradiography images (right).

Pearl No.	Macro image	Microradiography images	
		Side view	Facing view
1		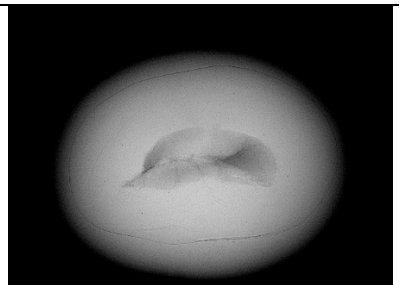	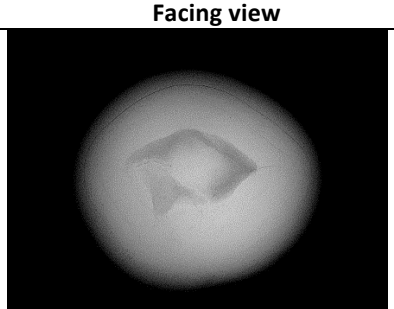
2		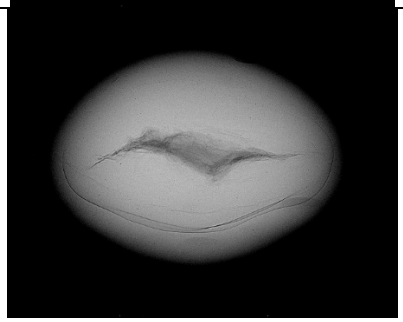	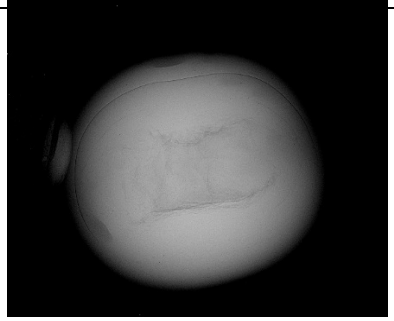
3		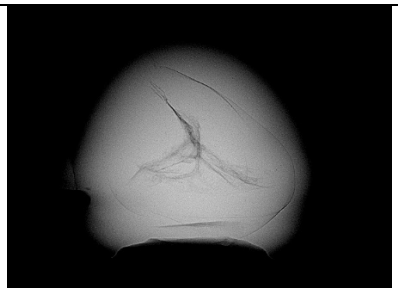	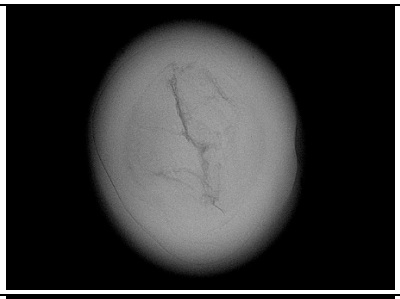
4		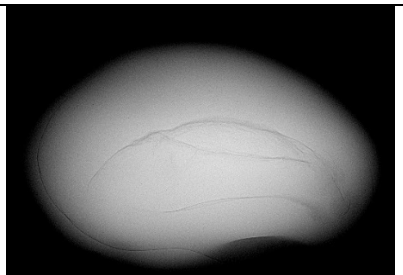	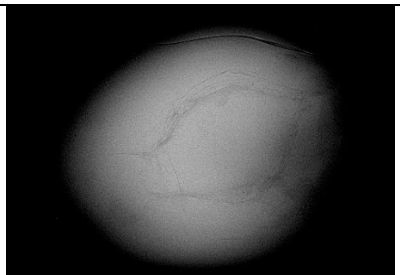
5		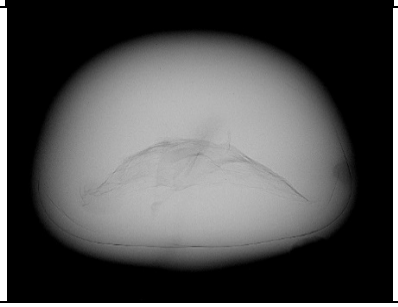	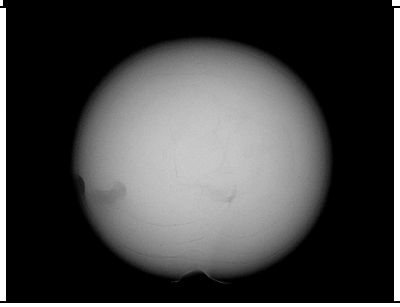

o

6			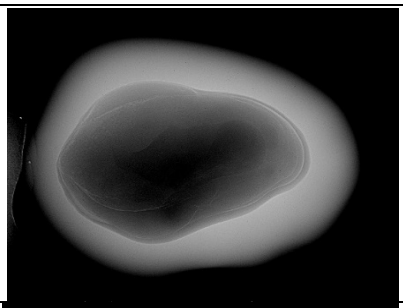
7		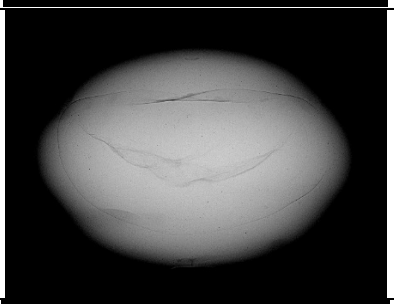	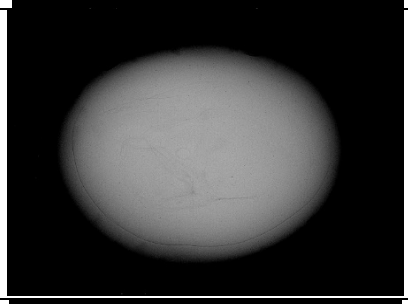
8		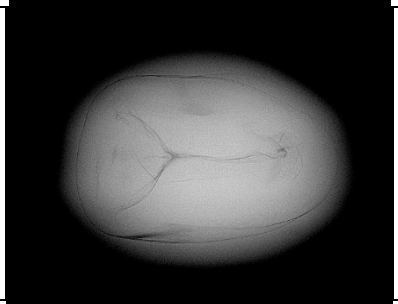	
9			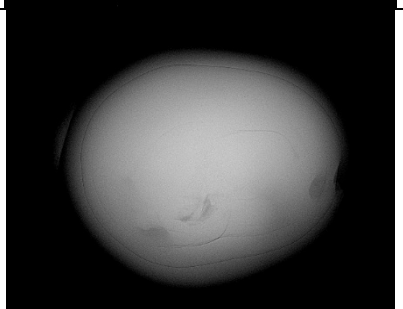
10		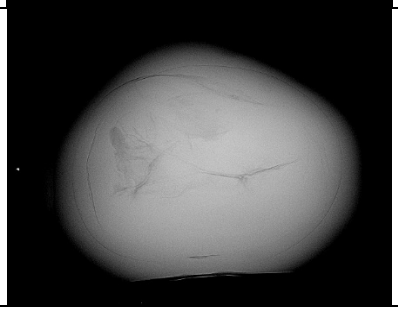	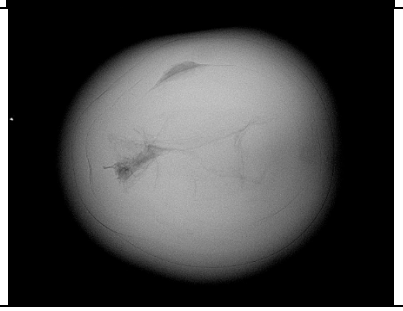

o

Pearls A and B were sawn in half to confirm their identification and observe/record the results from further work that could not be performed on the intact pearls. The inner features of sawn surfaces are shown in the photomicrographs in table 2. Pearl A showed a distinct boundary between the white pearl nucleus and the yellow nacre overgrowth, while the boundary between the aBC nucleus and overgrowth layers in pearl B was much harder to define owing to the similarity in colors between both components. Both pearls also showed features to one side of the nucleus that are typical of additional growth forms encountered in some pearls. These are often manifested as twin-type pearls with two points of origin that combine to form a single entity. In some cases, pearls (natural, bead cultured, or NBC) with multiple parts, all with their own core, may combine to form one baroque pearl. RTX images (table 2) show the internal structures in relation to the orientation of the photomicrographs shown. Along with an obvious nucleus demarcation boundary in pearl A, a complex linear-like structure was also visible in the center of the nucleus and an additional elongated structure (yellow arrows, table 2) was apparent in the twin part of the pearl. Furthermore, a “seed-like” satellite feature (red arrow, table 2) often associated with saltwater cultured pearls (Krzemnicki, 2010; Sturman et al., 2015; Nilpetploy et al., 2018) was also observed. Pearl B revealed a boundary/fold (white arrow, table 2) separating the pearl in two parts. The largest part showed an obvious FW aBC nucleus with a complex linear feature similar to that seen in pearl A, while the smaller part contained an irregular void typical of South Sea NBC pearls.

o

Table 2. Microphotography images (left) of one of the halves of each sample and the corresponding oriented microradiography image (right). Photos by Kwanreun Lawanwong.

Sample	Microphotography	Microradiography
Pearl A	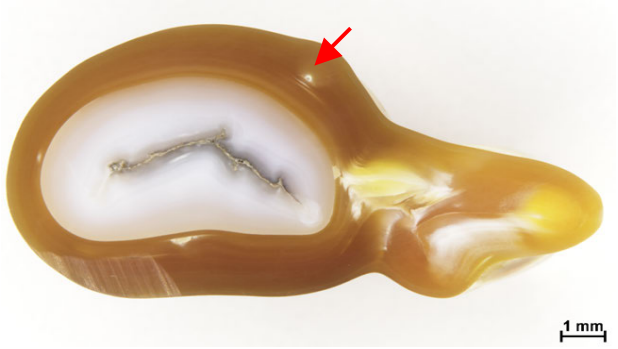	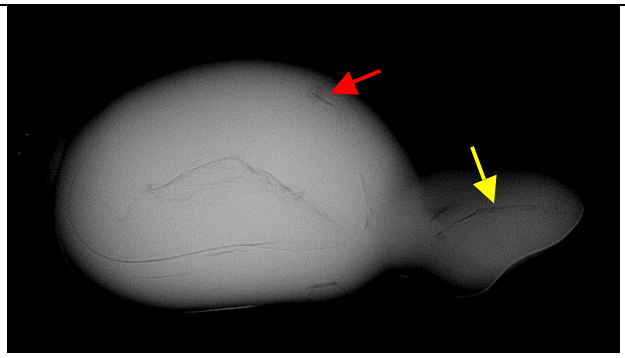
Pearl B		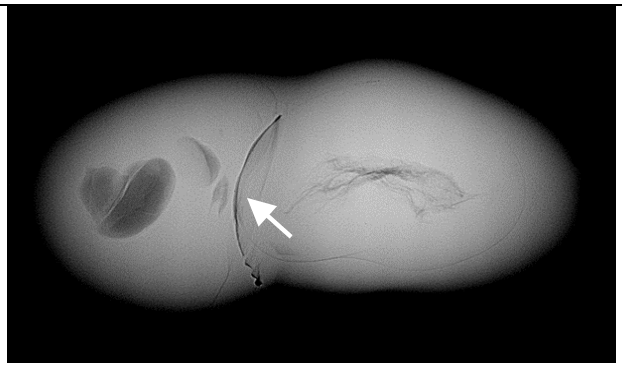

o

3.2 X-ray Computed Microtomography (µ-CT)

Even though the samples revealed fairly defined atypical bead demarcations, some of them were not quite as pronounced and so it was decided to perform µ-CT analysis to better discern their internal structures.

Three samples, pearls 3, 6, and 9 (table 1), were selected because their structures warranted further investigation**.** The µ-CT results in table 3 revealed more defined irregular nucleus outlines and complex linear features characteristic of FW NBC pearls in the center of each nucleus in pearls 3 and 9, while the absence of any clear growth features in the layers overgrowing the nucleus was also noted**.** The complex central linear feature in pearl 3 also contained some tiny white spots within it and also in the gap between the boundary **(**red arrows, table 3 and figures 3 and 4). Although such seeds are not diagnostic of a cultured origin, the authors' experience and the previous studies (Krzemnicki, 2011; Nilpetploy et al., 2018) have shown this to be more indicative of cultured pearl formation. Likewise, the complex linear feature in the center of pearl 9's nucleus, especially in the X and Z directions, is characteristic of FW NBC pearls (Krzemnicki, 2010), thus supporting the conclusion that a FW NBC pearl was used as a "bead" nucleus.

As was suspected from the RTX evidence, pearl 6 did not reveal an obvious demarcation line that would prove the presence of a similar FW NBC "bead" seen in all the other samples. Based on the features evident, especially the large void with organic-rich matter, this sample is an NBC pearl that was mistakenly included within the group. This shows just how easy it is to mix pearls of different identities based solely on their external appearance.

o

Table 3. The μ-CT slices of the three pearl samples in three different directions.

Pearl No.	μ-CT images		
	X-direction	Y-direction	Z-direction
3	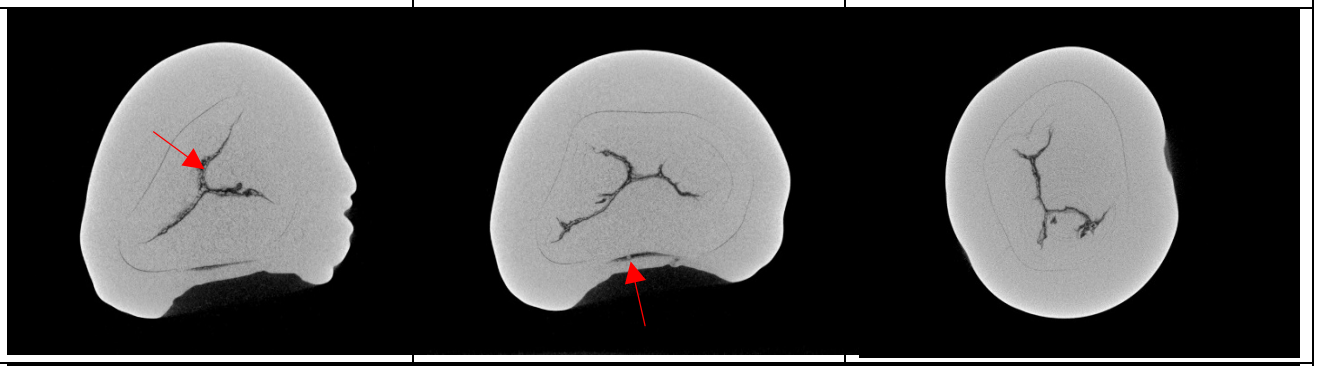		
6	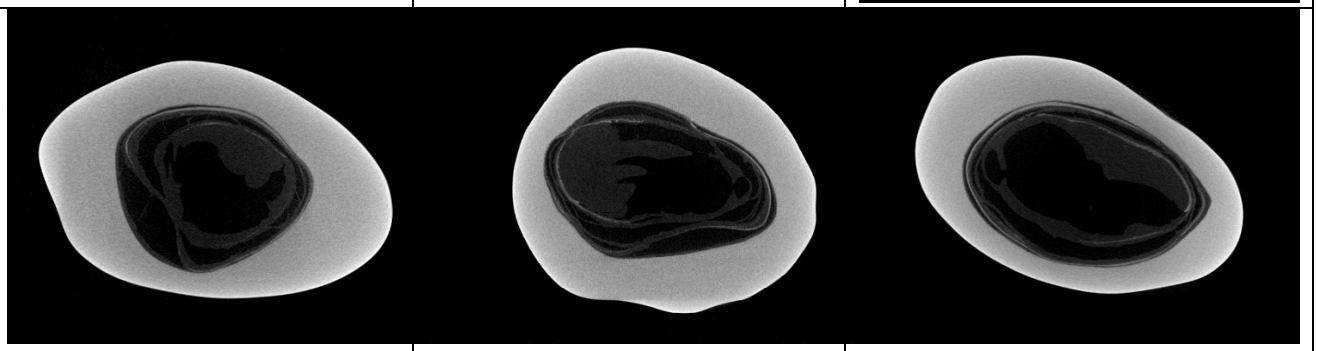		
9	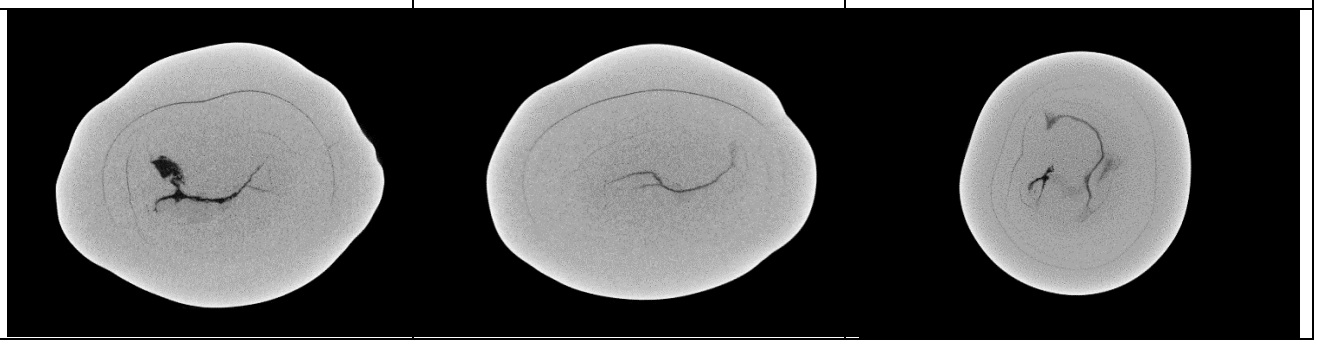		

o

Figure 3. A magnified µ-CT slice from the Y-direction of pearl 3 (table 3) showing a white seed-like structure in the central irregular void feature (see red arrow).

o

Figure 4. A magnified µ-CT slice from the Y-direction of pearl 3 (table 3) showing a white seed-like structure in the organic-rich demarcation area between the FW NBC pearl nucleus and the overlying SW pearl nacre (see red arrow).

3.3 Optical X-ray Fluorescence

The use of this analytical technique in pearl testing has been covered in the literature (Hänni et al., 2005; Kessrapong et al., 2017; Karampelas et al., 2019). However, in general the reactions of pearls to X-ray excitation fall into two groups; those that do not react (inert) and those that do react. The latter may be subdivided into two groups, the first showing very weak to weak reactions—some NBC and most saltwater BC pearls with a FW shell bead nucleus where the nacre is not too thick—and the second where the reaction is usually very strong and indicates a freshwater origin. The intensity of a pearl's fluorescence reaction is usually directly correlated to the level of manganese (Mn) within it. Since FW pearls usually contain more Mn than SW pearls, it is no surprise to see that FW pearls often show a stronger reaction. On the other hand, pearls that form in a saltwater environment are generally inert. As in most scenarios

o

there are exceptions to these rules, and it is possible to encounter both FW pearls with lower than usual (<100 ppmw) Mn levels that do not fluoresce strongly and rare examples of mixed-chemistry pearls (Sturman et al., 2019) that show reactions similar to those normally observed in FW pearls.

Eleven of the pearls in the group exhibited very weak to moderate X-ray fluorescence reactions, and only pearl 6 was inert. Unsurprisingly, the yellow and orangy yellow pearls showed the weakest reactions. This was due to a combination of the masking effect of their color, the tendency of white to cream pearls to show stronger reactions, and the nacre thickness of the layers surrounding the FW nucleus in each. Pearl 6 was inert because it is an NBC pearl and thus lacks the FW nucleus observed in the remaining samples.

The two pearls selected for sawing revealed distinct reactions that were not so apparent in their intact forms. The FW NBC pearl nucleus in each produced weak to moderate reactions through the SW nacre layers overgrowing them, with pearl A displaying yellow/orange color and pearl B displaying a yellowish green color (figure 5B). The reactions of the sawn pieces were much more revealing and showed striking differences between the FW and SW components (figure 5D).

X-ray fluorescence is an extremely sensitive and useful test available to gemologists. The results obtained from both sawn pearls showed that the nucleus in pearl A fluoresced a yellow color similar to that seen externally prior to sawing, and that the nucleus of pearl B fluoresced to a similar degree, only with a greenish hue. These results supported the identity obtained from the RTX work and helped confirm that they were aBC pearls with a FW NBC pearl used as the nucleus.

o

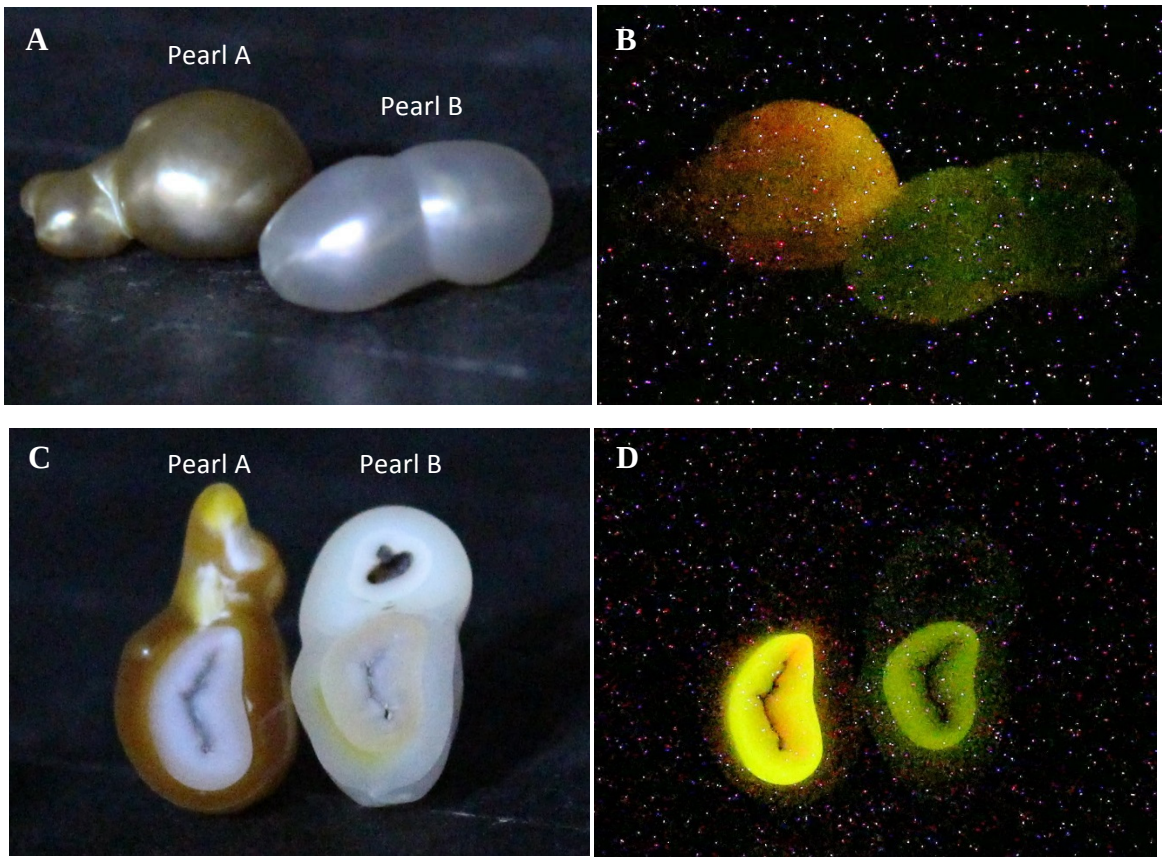

Figure 5. Images of the two pearl samples selected, showing them as whole pearls (A) and their reactions under optical X-ray fluorescence (B). The inner surfaces of two halves of each of the pearls are shown in LED lighting (C) and under X-ray excitation (D).

3.4 Raman and PL Spectroscopy

Seven pearls from the group exhibited a yellow to strong yellow coloration, and each of them was also examined with Raman and PL spectroscopy to confirm their color origin. All revealed spectra consistent with naturally colored *Pinctada maxima* (gold-lipped) shell and pearls studied previously (Elen, 2001; Zhou et al., 2012; Cartier and Krzemnicki, 2016). Two different areas, the outer surface and similarly colored layers overgrowing the nucleus of sawn pearl A, were examined to compare the results. The Raman spectra showed aragonite peaks at 701/705 (doublet), 1085, and 1462 cm^{-1} (Urmos et al., 1991), as well as pigment-related features of various intensities at approximately 1388 and 1542 cm^{-1} (Cartier and Krzemnicki, 2016) related to the color saturation within the areas tested. This can clearly be seen in figure 6, where the spectrum obtained from the inner area shows more pronounced features at approximately 1388 and 1542 cm^{-1} than those in the spectrum obtained from the outer surface. The PL spectra of all samples, including pearl A, exhibited a domed form typical of previous studies (Zhou et al., 2012; Kwak et al., 2016) with a maximum at around 650 nm. No other obvious features were noted, save one at 544 nm associated with the dominant aragonite peak

o

observed at 1085 cm^{-1} in the Raman spectra. In keeping with the Raman spectra, the PL result from the inner surface of pearl A showed higher fluorescence, while the spectrum from the outer surface revealed much weaker fluorescence (figure 7). The differences in the intensities and spectral features seen may be explained by the more saturated color of the inner layers compared to the lighter-colored outer nacre.

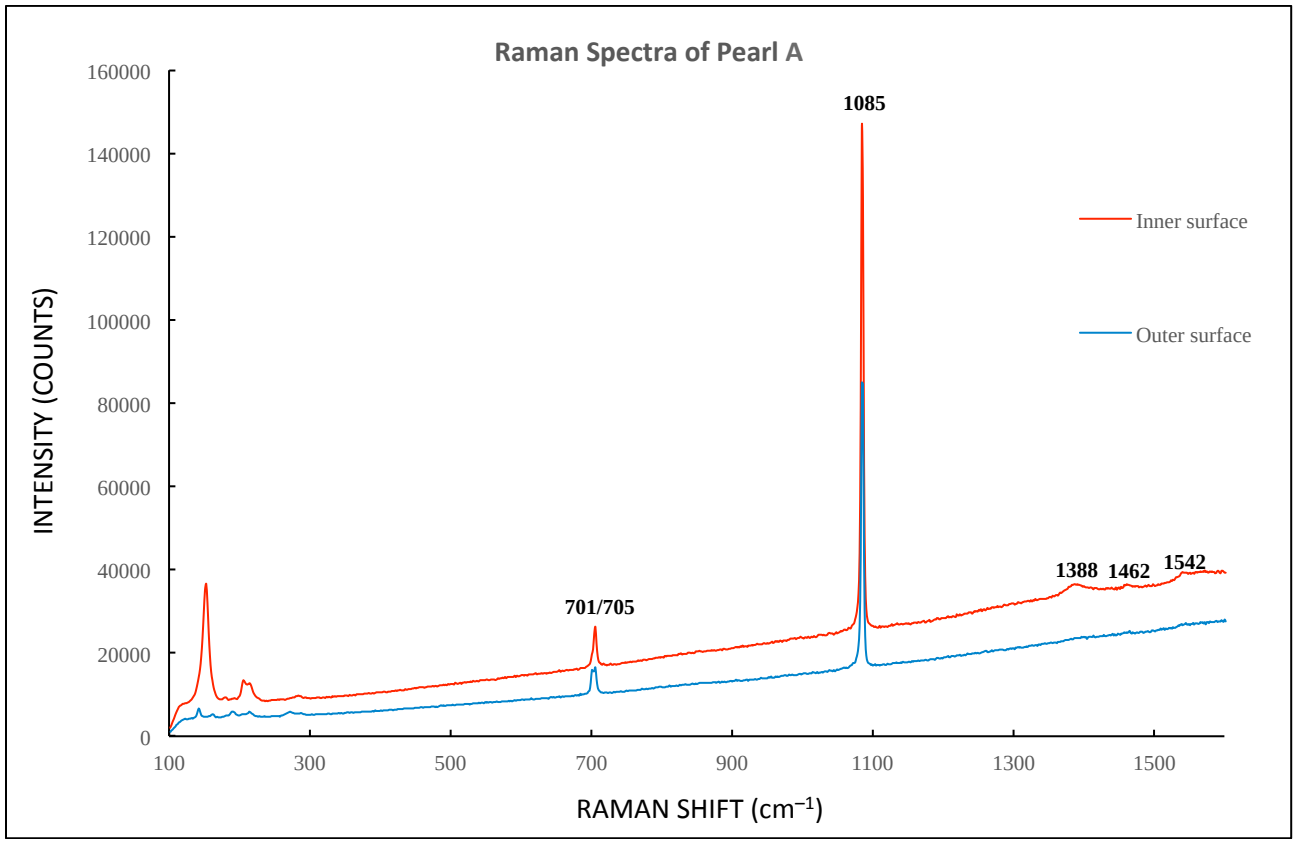

Figure 6. Raman spectra of pearl A, outer surface (blue line) and inner surface (red line), showing aragonite peaks at 701/705, 1085, and 1462 cm^{-1}. The pigment-related features at 1388 and 1542 cm^{-1} are clearly visible in the spectrum collected from the more saturated color layers surrounding the nucleus within the pearl.

o

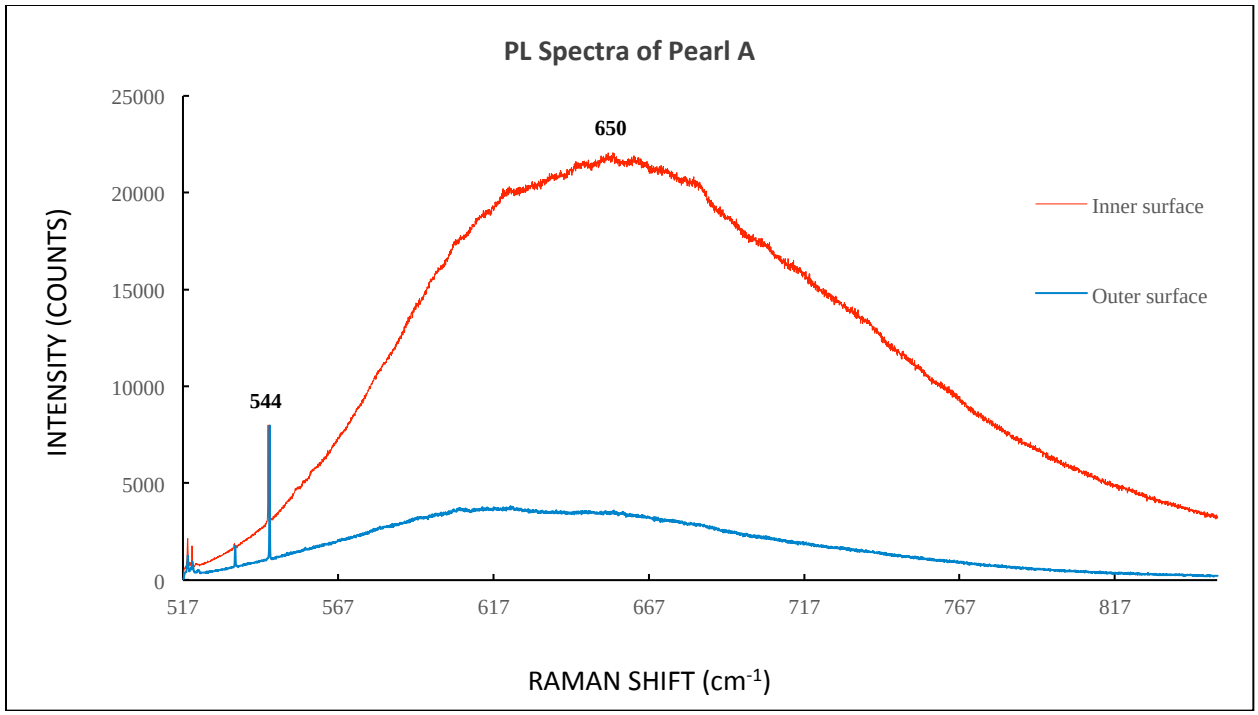

Figure 7. Photoluminescence spectra of pearl A, outer surface (blue line) and inner surface (red line), showing domed spectra with a maximum at approximately 650 nm. The feature at 544 nm is associated with the aragonite peak at 1085 cm^{-1} in the Raman (figure 6). Note the higher fluorescence exhibited by the inner surface.

3.5 Visible Spectrophotometry

The UV-Vis spectra obtained from the external surfaces of the seven "golden" samples revealed an area of lower reflectance between approximately 330 and 460 nm, higher reflectance between approximately 480 and 700 nm, and a high-reflectance feature at approximately 310 nm, together with a low-reflectance feature at 280 nm (figure 8). All the features are consistent with those observed in known samples of naturally colored yellow *Pinctada maxima* samples the authors have examined in GIA's database and that have also been recorded in prior literature (Elen, 2001; Cartier and Krzemnicki, 2016). The authors were unable to obtain spectra of high enough quality from the inner surfaces of both sawn samples to reproduce here.

o

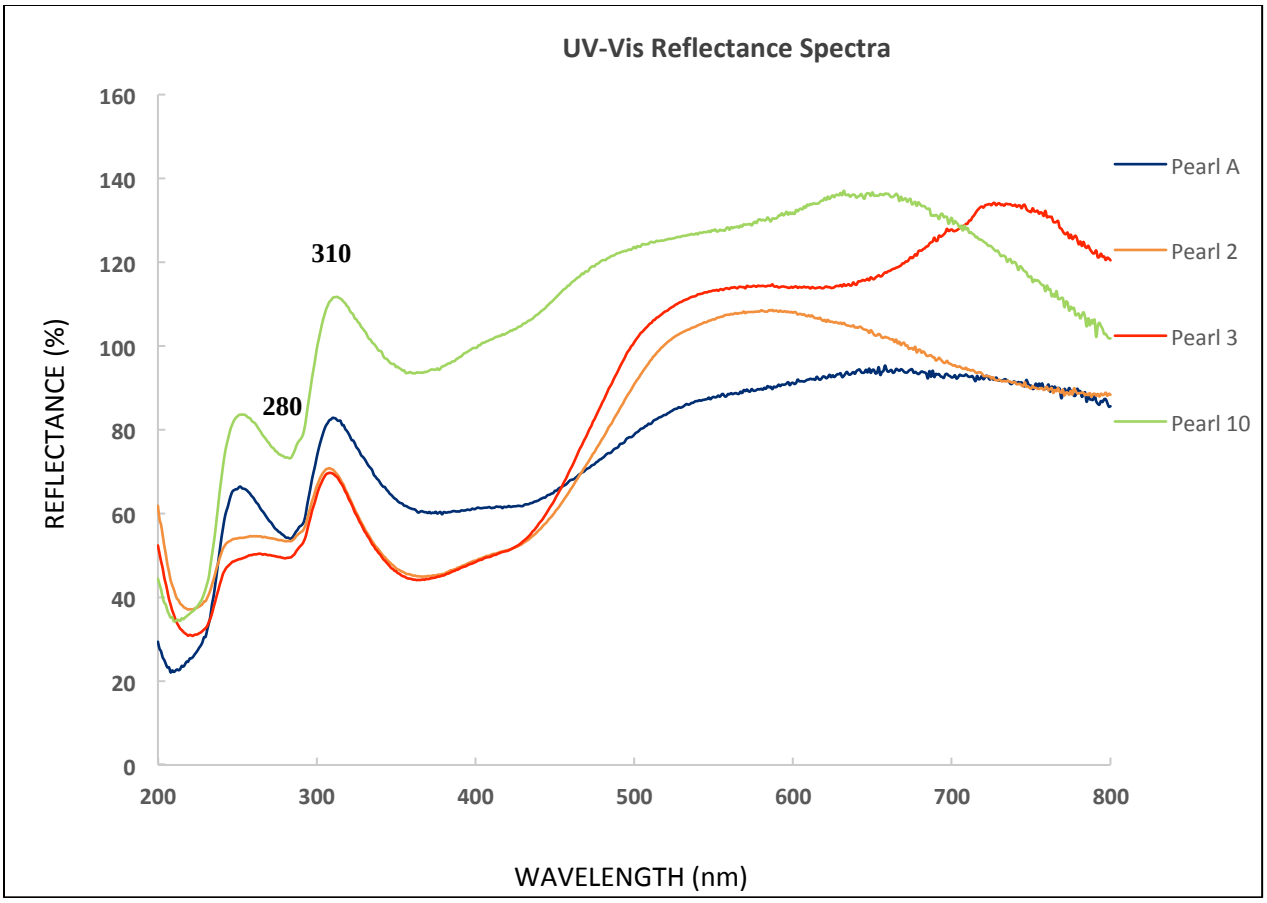

Figure 8. The UV-Vis reflectance spectra of four representative pearls (A, 2, 3, and 10) showing lower-reflectance features at 330–460 nm as well as a higher-reflectance feature at 310 nm. Pearl 10 exhibited the lightest color and pearl 2 the most saturated coloration.

3.6 LA-ICP-MS

Pearls from FW and SW environments are separated not only by the optical X-ray fluorescence method described previously. The quantities of the trace elements—especially manganese (Mn), strontium (Sr), and barium (Ba)—present within shells and pearls necessary to make the separation may be detected using energy dispersive X-ray (EDXRF) spectrometry and/or laser ablation–inductively coupled plasma–mass spectrometry (LA-ICP-MS). The latter method of analysis is useful when more detailed results are needed, though the analysis spot is only around 40 microns across and in depth (Abduriyim, 2018; Karampelas et al., 2019). Higher quantities of Sr indicate a pearl formed in a saltwater environment, while higher quantities of Mn indicate a freshwater environment.

The majority of saltwater pearls tested in GIA laboratories possess Sr levels between 1,000 and 2,000 ppmw, while in freshwater pearls the quantities may fall below detection limits (BDL) to 200 ppmw at most. A higher Mn content is the main indicator of formation in a freshwater environment, with the usual range from 100 to 5,000 ppmw. The EDXRF results on the external

o

surfaces of the pearls studied proved they originated from a SW environment. However, since the various X-ray-based techniques applied prior to the LA-ICP-MS analysis proved that a FW NBC pearl nucleus existed in 11 of the samples, the decision was taken to cut two of the samples in half to study their inner chemistry results and fluorescence reactions. The findings of the LA-ICP-MS analysis on one half from each pearl (figures 9 and 10) proved that the NBC nuclei used were FW in nature while the overgrowth layers were SW, per the exterior EDXRF analysis originally undertaken.

A total of 58 laser ablation spots were positioned across the inner surface of pearl A (figure 9) in a line from the exterior surface of one side (spot #1) to the opposite side (spot #58). The results showed different quantities of Sr and Mn between the two nacreous components examined, with the spots numbered 1–11 and 45–58 within the yellow nacre revealing higher concentrations of Sr than Mn, as expected for SW material, while spots 12–44 showed higher concentrations of Mn than Sr (figure 9), characteristic of FW material.

Figure 9. Macro image of pearl A showing 58 LA-ICP-MS spots traversing the SW yellow-orange nacre and the inner FW white nucleus. The differences in the quantities of Mn and Sr detected in the spots across the two areas are shown in figure 11. Photo by Sasithorn Engniwat.

o

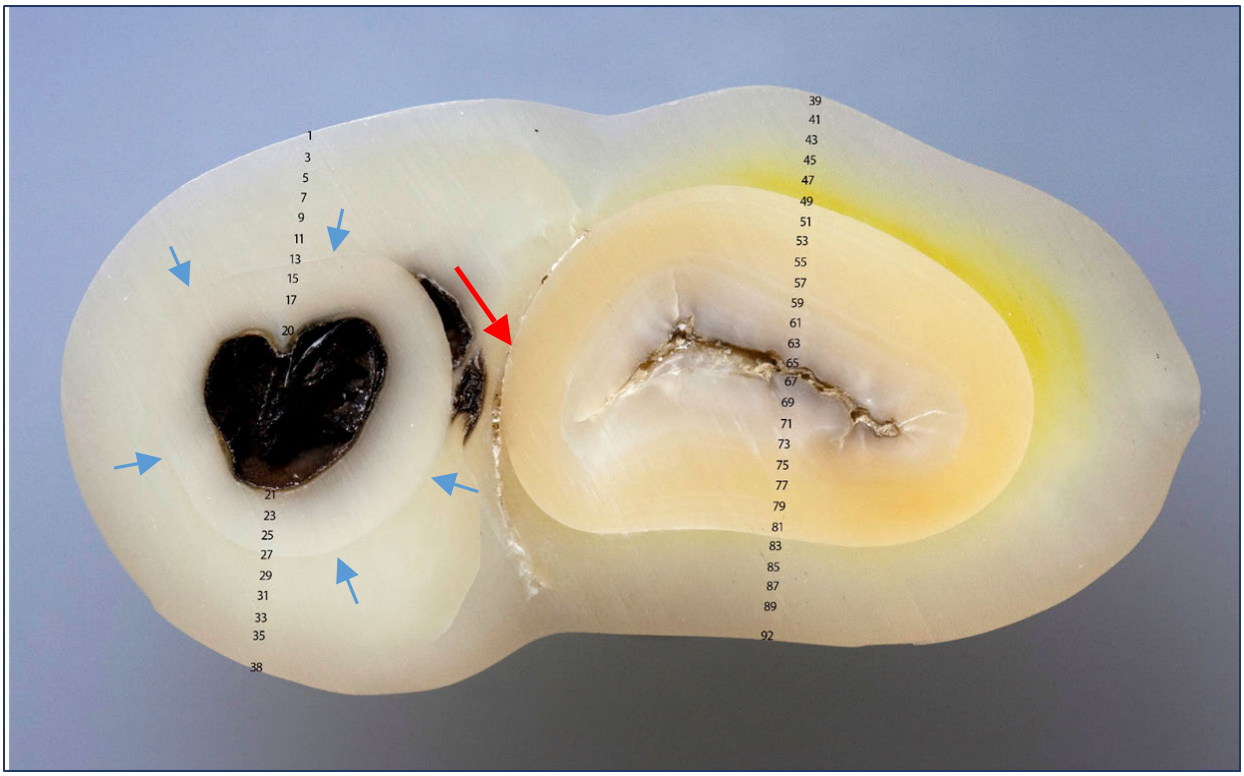

Figure 10. Macro image of pearl B showing a total of 92 LA-ICP-MS spots traversing the inner surface. The differences in the quantities of Mn and Sr detected in the spots across the two areas are shown in figure 12. Photo by Sasithorn Engniwat.

The LA-ICP-MS results on pearl B were as clear as those obtained from pearl A. The different quantities of Sr and Mn within different areas of the saltwater nacre overgrowth and freshwater nucleus were readily apparent. A total of 92 laser ablation spots were positioned in two lines across two areas of the inner surface. The results obtained from spots 1–49 and 83–92 proved that these areas formed in a saltwater environment, while spots 50–82 within the pearl's nucleus (cream color in figure 10) matched with the chemistry expected for a freshwater environment. The quantity of Sr was higher than Mn in the nacre overgrowth area and in the solid nacre area of the twin (spots 1–38) around the void to the left of the boundary line (red arrow in figure 10), while the quantity of Mn was higher than Sr in the freshwater nucleus (figure 10). Initially there was some concern that the area around the void, the white ring immediately surrounding it (see blue arrows), could be another aBC nucleus, but the LA-ICP-MS results confirmed that the chemistry was SW and hence more likely related to the formation of the layers around the FW nucleus, or was a separate NBC ("keshi") formation that merged with the SW layers surrounding the FW nucleus as the former aBC pearl developed (Krzemnicki et al., 2011; Nilpetploy et al., 2018).

o

Plotting the LA-ICP-MS spots (figures 11 and 12) clearly shows that the Mn levels of the FW areas is considerably higher in the two nucleus areas, while the corresponding Sr levels drop significantly, as would be expected in FW materials. The opposite is true when the SW areas are viewed.

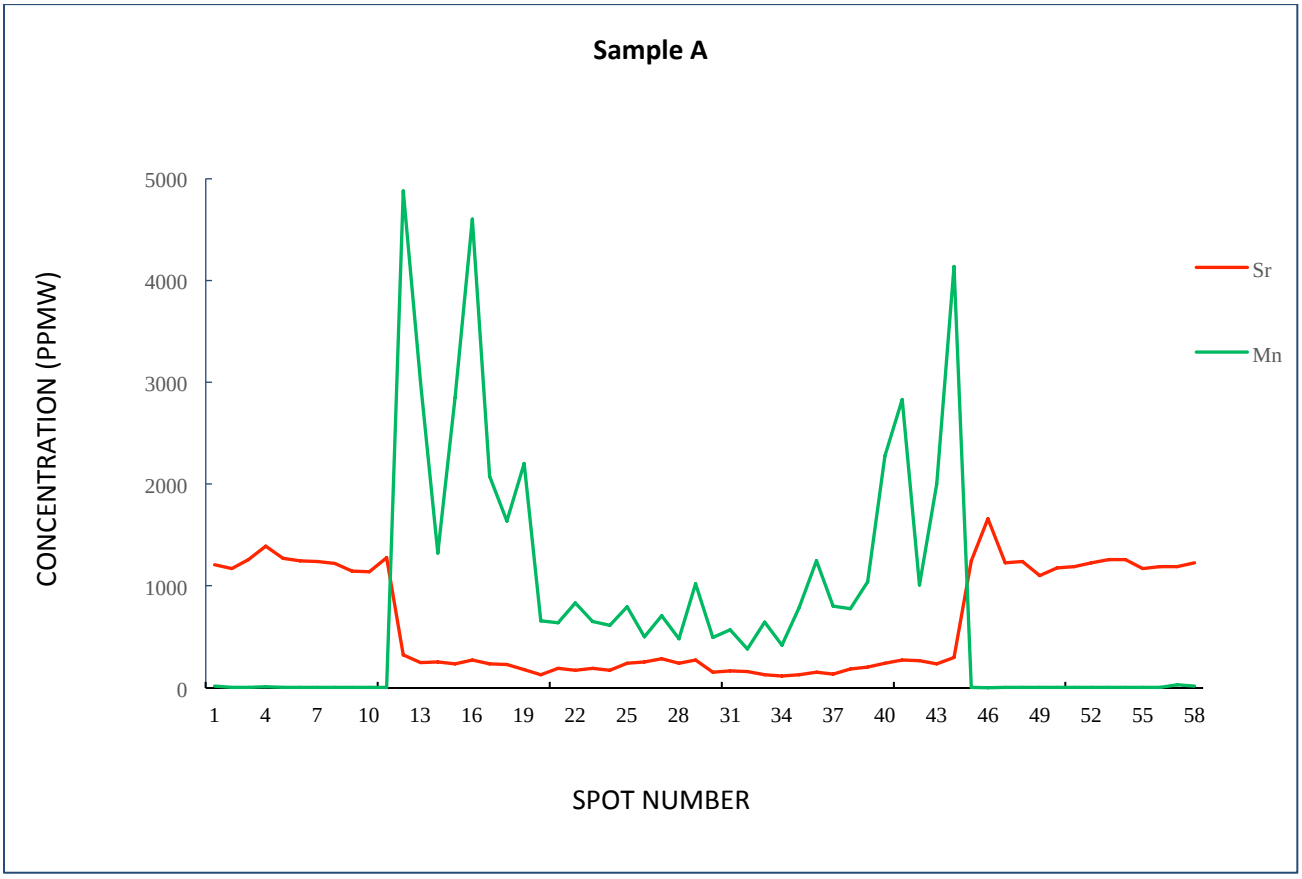

Figure 11. Pearl A showing the quantities of Mn and Sr (ppmw) in relation to the LA-ICP-MS spots tested (1–58) traversing the pearl (figure 9). Spots 12–44 fall within the freshwater nucleus and correspond to higher Mn and lower Sr levels.

o

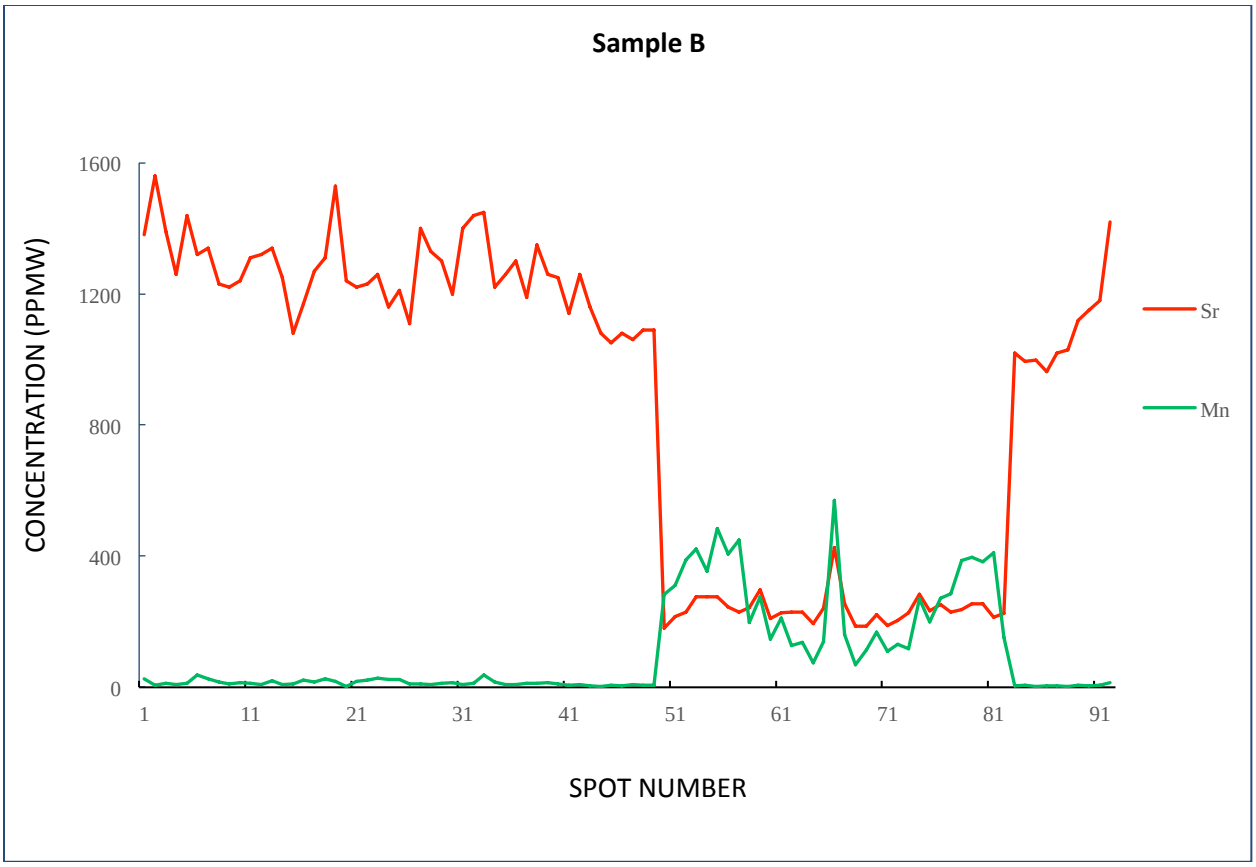

Figure 12. Pearl B showing the quantities of Mn and Sr (ppmw) in relation to the LA-ICP-MS spots tested (1–92) traversing the pearl (figure 10). Spots 50–82 fall within the freshwater nucleus which correspond to higher Mn and lower Sr levels.

4. Conclusion

The overall appearance of the 12 South Sea pearls loaned for this work indicated that they were probably cultured. Their external appearance was similar, with only their colors showing significant difference. Yet the overall features were consistent with bead cultured or non-bead cultured pearls from the *Pinctada maxima* mollusk. Standard laboratory pearl identification methods, primarily RTX analysis, revealed that 11 samples were aBC pearls, as claimed by the supplier, while one showed a structure characteristic of NBC pearls. The 11 aBC pearls showed a demarcation boundary typical of such pearls between the outer surfaces of the freshwater pearl nuclei and the inner surfaces of the overlying saltwater nacre overgrowth. However, the definition of the boundary between the two components was not always obvious, and thus some samples required further µ-CT analysis. It was interesting to note that the more elongated baroque shape pearls, such as the two selected for further detailed analyses (pearls A and B), exhibited more pronounced demarcation boundaries.

This was part of the reason why both samples were examined further using a variety of techniques. Microradiography initially revealed internal structures indicating a FW NBC pearl

o

was used as a nucleus. Their optical X-ray fluorescence reactions also indicated that the nuclei were FW origin, since the strength of the reaction was greater than that normally observed in pearls from a SW environment. Destructive testing was subsequently applied to samples A and B in order to reveal their internal structures more clearly. The actual boundaries in relation to the RTX results were then clearly visible, and the optical X-ray fluorescence reactions were extremely telling and allowed the unquestionable separation of the two different environmental components. Their defined reactions also tallied precisely with the trace element chemistry data subsequently collected from their inner surfaces. Even though standard gemological testing is usually enough to identify such pearls, the sawing of the two samples proved to be a useful exercise to carry out for the sake of scientific examination and led to even greater clarity.This study helped in clarifying the characteristic structures expected in this type of atypical bead cultured pearl and in distinguishing it from other entirely saltwater atypical bead cultured pearls (both the nucleus and overgrown layers formed in SW) as well as SW non-bead cultured pearls. The sawing helped further our understanding of the pearls, and the subsequent LA-ICP-MS analyses proved to be a powerful technique that allowed us to trace the chemistry across the two formation environments. When destructive testing is not an option, some pearl samples might exhibit questionable RTX results where the demarcation between the two components is unclear, and thus further µ-CT examination may be necessary.

Destructive testing naturally has its drawbacks and was only applied in this research with the vendor's full authorization since it ultimately changes the pearls' shape, luster, and weight. A pearl's internal structure is obviously damaged by the process as well. LA-ICP-MS spots only affect the surface condition to a small degree and result in very small partial drill holes in the tested areas. The weight loss is insignificant, and thus the method is acceptable in pearl testing when necessary. Virtually all pearl testing techniques carried out by gemological laboratories are non-destructive. Methods such as RTX, optical X-ray fluorescence, and µ-CT very rarely impact the appearance of any pearls and are the only techniques needed to identify atypical bead cultured South Sea pearl nucleated with freshwater non-bead cultured pearls.

5. About the Authors

Mr. Kessrapong and Ms. Lawanwong are analytics technicians in the pearl identification department at GIA in Bangkok.

6. Acknowledgments

The authors appreciate the cooperation of Mr. Devchand Chodhry of Orient Pearl (Bangkok) Limited, who loaned the samples to GIA and allowed gemologists at GIA's Bangkok laboratory to conduct destructive testing on the two selected samples. Other members of GIA's pearl identification team, field gemology, and colored stone teams are also thanked for their assistance in collecting data and producing this article.

o

References

Abduriyim A. (2018) Cultured pearls from Lake Kasumigaura: Production and gemological characteristics. *G&G*, Vol. 54, No. 2, pp. 166–183, http://dx.doi.org/10.5741/GEMS.54.2.166

Cartier L.E., Krzemnicki M.S. (2016) Golden South Sea cultured pearls: Cultivation steps & Gemological investigations. *The Journal of Gemological Association of Hong Kong*, Vol. 37, pp. 16–21.

Elen S. (2001) Spectral reflectance and fluorescence characteristics of natural-color and heat-treated "golden" South Sea cultured pearls. *G&G*, Vol. 37, No. 2, pp. 114–123, http://dx.doi.org/10.5741/GEMS.37.2.114

Gemological Institute of America (2011) *Pearls*. The Berne Convention, United States of America.

Hänni H.A., Kiefert L., Giese P. (2005) X-ray luminescence, a valuable test in pearl identification. *Journal of Gemmology*, Vol. 29, No. 5/6, pp. 325–329.

Hänni H.A., Krzemnicki M.S., Cartier L.E. (2010) Appearance of new bead material in cultured pearls. *Journal of Gemmology*, Vol. 32, No. 1-4, pp. 31–37.

Homkrajae A., Sun Z., Blodgett T., Zhou C. (2019) Provenance discrimination of freshwater pearl by LA-ICP-MS and linear discrimination analysis (LDA). *G&G*, Vol. 55, No. 1, pp. 47–60, http://dx.doi.org/10.5741/GEMS.55.1.47

Hsu T., Zhou C., Homkrajae A., Ho J.W.Y., Yazawa E., Padua P. (2016) Freshwater pearling in Tennessee. *GIA Research News*, https://www.gia.edu/gia-news-research/freshwater-pearling-tennessee

Karampelas S., Mohamed F., Abdulla H., Almahmood F., Flamarzi L., Sangsawong S., Al-Alawi A. (2019) Chemical characteristics of freshwater and saltwater natural and cultured pearls from different bivalves. *Minerals*, Vol. 9, No. 357, pp. 1–20.

Kessrapong P., Lawanwong K., Sturman N. (2017) *Pinctada maculata* (Pipi) bead-cultured blister pearls attached to their shells. *GIA Research News*, April 25, https://www.gia.edu/gia-news-research/pinctada-maculata-bead-cultured-blister-pearls-shells

Kessrapong P., Lawanwong K. (2018) Atypical "bead"-cultured *Pinctada maxima* pearls nucleated with freshwater non-bead-cultured pearls. Proceedings of the 2018 GIA International Gemological Symposium, *G&G*, Vol. 54, No. 3, pp. 294–295.

o

Krzemnicki S.M., Müller., Hänni H.A., Gut H.P., Düggelin M. (2011) Tokki pearls: Additional cultured pearls formed during pearl cultivation: External and internal structures. *32nd International Gemmological Conference 2011*, pp. 1–14.

Krzemnicki S.M., Friess D.S., Chalus P., Hänni H.A., Karampelas S. (2010) X-ray computed microtomography: Distinguishing natural pearls from bead and non-beaded cultured pearls. *G&G*, Vol. 46, No. 2, pp. 128–134, http://dx.doi.org/10.5741/GEMS.46.2.128

Kwak K., Lee J., Jeong E. (2016) Identification of dyed golden South Sea pearls using UV-Vis and PL tests. *The Journal of the Gemological Association of Hong Kong*, Vol. 37, pp. 58–61.

Nilpetploy N., Lawanwong K., Kessrapong P. (2018) Non-bead cultured pearls from *Pinctada margaritifera*. *GIA Research News*, April 27, https://www.gia.edu/gia-news-research/non-bead-cultured-pearls-from-pinctada-margaritifera

Scarratt K., Sturman N., Tawfeeq A., Bracher P., Bracher M., Homkrajae A., Manustrong A., Somsa-ard N., Zhou C. (2017) Atypical "beading" in the production of cultured pearls from Australian *Pinctada maxima*. *GIA Research News*, https://www.gia.edu/gia-news-research/atypical-beading-production-cultured-pearls-australian-pinctada-maxima

Strack E. (2006) *Pearls*. Rühle-Diebener-Verlag, Baden-Baden, Germany.

Sturman N. (2009) The microradiographic structures of non-bead cultured pearls. *GIA Research News*, https://www.gia.edu/gia-news-research-NR112009

Sturman N., Homkrajae A., Manustrong A., Somsa-ard N. (2015) X-ray computed microtomography (µ-CT) structures of known natural and non-bead cultured *Pinctada maxima* pearls. *Proceedings of the 34th International Gemmological Conference*, Vilnius, Lithuania.

Sturman N., Bergman J., Poli J., Homkrajae A., Manustrong A., Somsa-ard. N. (2016) Bead-cultured and non-bead-cultured pearls from Lombok, Indonesia. *G&G*, Vol. 52, No. 3, pp. 288–297, http://dx.doi.org/10.5741/GEMS.52.3.288

Sturman N., Otter L.M., Homkrajae A., Manustrong A., Nilpetploy N., Lawanwong K., Kessrapong P., Jochum K.P., Stoll B., Götz H., Jacob D.E. (2019) A pearl identification challenge. *G&G*, Vol. 55, No. 2, pp. 229–243, http://dx.doi.org/10.5741/GEMS.55.2.229

Urmos J., Sharma S.K., Machenze F.T. (1991) Characterization of some biogenic carbonates with Raman spectroscopy. *American Mineralogist*, Vol. 76, pp. 641–646.

o

Zhou C., Homkrajae A., Ho J.W.Y., Hyatt A., Sturman N. (2012) Update on the identification of dye treatment in yellow or “golden” cultured pearls. *G&G*, Vol. 48, No. 4, pp. 284–291, http://dx.doi.org/10.5741/GEMS.48.4.284

o